KSCE Journal of Civil Engineering (2022) 26(12):5372-5383
DOI 10.1007/s12205-022-1664-2

pISSN 1226-7988, eISSN 1976-3808
www.springer.com/12205

Tunnel Engineering

Analysis and Modeling of Longitudinal Deformation Profiles Considering the Reinforcement Effect of Tunnel Face in Weak Rocks

Zhilong Wang[a], **Mingnian Wang**[a], **and Dagang Liu**[a]

[a]*Key Laboratory of Transportation Tunnel Engineering, Ministry of Education, Southwest Jiaotoug University, Chengdu, Sichuan 610031, China*

ARTICLE HISTORY

Received 15 May 2022
Accepted 17 July 2022
Published Online 22 September 2022

KEYWORDS

Longitudinal deformation profiles
Tunnel face
Convergence-confinement method
Support design
Extrusion deformation

ABSTRACT

Convergence-confinement method (CCM) has become a common method for tunnel design due to its simplicity and practicality. The ground reaction curve (GRC), the support characteristic curve (SCC) and the longitudinal deformation profile (LDP) are all considered in this method. One of these is the LDP, which serves as a unique identifier for the location of the tunnel support. The installation point of the tunnel support is one of the most important outcomes of the method. LDP is more impacted by the reinforcement of the tunnel face. However, more existing LDP calculation methods do not consider the reinforcement of the tunnel face. A study on methods for calculating LDP considering the tunnel face reinforcement was carried out to address this constraint of CCM. Firstly, the transformation of tunnel face extrusion deformation and pre-convergence deformation at the tunnel face is realized in accordance with equivalent volume. Then a model of LDP with the tunnel face extrusion deformation as the variable was established considering the tunnel face reinforcement effect. The proposed model's accuracy is assessed in comparison with other typical models. We conclude with parametric analyses concerning the tunnel face reinforcement's effects on the point of support installation, as well as convergence deformation of the tunnel. By taking into account tunnel faces' reinforcement effects, tunnel support design can be more accurate, and the construction costs can be reduced.

1. Introduction

Building tunnels in weak rock masses such as fractured rock, weathered rock and soft rock has traditionally been a difficult task in tunneling. Advances in design methods for weak rock tunneling are an important prerequisite for ensuring the stability of weak rock tunnels. With the development of rock mechanics and the application of anchor spraying support, a modern support theory based on rock mechanics theory and considering the joint action of the rock mass and the tunnel support has been gradually formed. The basic idea of this theory is considering the rock mass and the tunnel support as a whole, interacting and carrying together, thereby maximizing the rock mass's self-supporting capability and obtaining the maximum economic effect. Calculation models and design approaches based on current support theory have been devised one after the other to analyze rock mass interactions with support, of which the CCM (Fenner, 1938) is one of the most representative design methods. This design method focuses on the rock behavior under constraint pressure, which considers the spatial effect on the tunnel face, the self-supporting properties of the rock mass, and the point of the tunnel support installed as tunnels are excavated, and it is composed of three main parts, namely the LDP which reflects the relationship between the tunnel wall displacement and the position of the tunnel face, the GRC which reflects the relationship between the internal pressure and the displacement (convergence) of the rock mass and the SCC which reflects the relationship between the deformation and the tunnel support pressure (Oke et al., 2018).

Research has been conducted on the GRC by several researchers (Alejano et al., 2009; Wang and Nie, 2010; Zhang et al., 2012; Cui et al., 2019; Kabwe et al., 2019; Zhang et al., 2019; Zhou et al., 2020). And the SCC was firstly proposed by Hoek and Brown (Hoek, 1980) of support structures for various types, and then other researchers explored this further (Carranza-Torres and

CORRESPONDENCE Dagang Liu 805294490@qq.com Key Laboratory of Transportation Tunnel Engineering, Ministry of Education, Southwest Jiaotoug University, Chengdu, Sichuan 610031, China

ⓒ 2022 Korean Society of Civil Engineers

Fairhurst, 2000; Oreste, 2003; Oreste, 2008). Since the LDP determines the point of the support installed, it has a crucial influence on the support design. Therefore, the main focus of this paper is LDP.

Panet (1995) (Panet, 1995) presented the formal LDP to describe the position of tunnel support installation without the necessity tunnel support thorough numerical method. And tunnel designers can rapidly see both the appropriate for installing support for the tunnel face and the support reaction thanks to Panet's expertise. And more LDP calculation models have been proposed in the later period. Researchers have come up with a variety of solutions to the LDP. The current research methods on LDP can be categorized into two types, specifically, the empirical method and the numerical method. There are relatively few LDP calculation equations using empirical methods, and the representative ones are mainly proposed by Lee (1994) and E. Hoek. But the models for LDP using the numerical methods have been proposed by many researchers, most of which rely on elastics (Unlu and Gercek, 2003), elastic-perfectly plastic (Alejano et al., 2009; Vlachopoulos and Diederichs, 2009; Basarir et al., 2010), elastic-brittle plasticity (Carranza-Torres and Fairhurst, 2000) and strain-softening behavior of rock mass (Song et al., 2020). It is evident that more and more research has been conducted on LDP. Among them, one model proposed by Vlachopoulos and Diederichs (Vlachopoulos and Diederichs, 2009) (denoted in this paper as V-D (09)) is the most typical and widely used. V-D (09) assumed perfectly plastic conditions with no dilation. The inputs for the V-D (09) depend on the GRC's solution.

However, none of the existing methods for the LDP considers the reinforcement effect of the tunnel face. In the case of improving the tunnel's overall stability, more tunnel faces are reinforced in weak rocks, especially in the poor quality ground, squeezed, or unstable ground (Cantieni et al., 2011; Barla, 2016). Deformation of a tunnel's core is what caused the entire process of deformation, as the experience shows (Lunardi, 2008). And it is also possible to reduce tunnel deformation by artificially controlling the strength and stiffness of the tunnel face, i.e., by considering the advanced core as a new tool for long-term and short-term tunnel stabilization (Lunardi, 2008). The LDP is necessarily changed after the tunnel face is reinforced. Then, the point of the support installed is affected. And it has a large impact on the support design.

Taking tunnel face reinforcement into account, this study presents a solution to overcome these limitations. Firstly, the transformation of tunnel face extrusion deformation and pre-convergence deformation is realized based on the principle of equivalent volume. Then, a model for calculating LDP considering the tunnel face extrusion deformation was established based on the basic form of the V-D (09) formula. And the rationality of the computational model in this paper is verified through case studies.

2. Problem Description

A study is conducted on the deformation law of rock mass during tunnel excavation by Lunardi (2008) using laboratory tests, theoretical analysis, and numerical calculation. These results suggested that deformations of the tunnel's advanced core were ultimately responsible for all of its deformations (extrusion, pre-convergence, convergence), as shown in Fig. 1, and due to its rigidity, the core was a key factor in ensuring stability of tunnels both in the short and long run.

Tunnel excavation is a three-dimensional mechanical problem (Luo et al., 2018), and the tunnel support design must consider both the interaction between the tunnel support and the rock mass and the spacing effect of the rock mass at the tunnel face. The CCM is one of the most design method that the ground response of the tunnel excavation and the effect of tunnel support installations can be assessed. The LDP's goal is to pinpoint the exact spot where the support will be deployed. The method's major practical effect is the establishment of a point of support.

The schematic diagram of the rock-support interaction under different LDPs is shown in Fig. 2 l_a and l_b are the LDP with and without tunnel face reinforcement, respectively. Assuming that the tunnel support is installed at the tunnel face, the pre-convergence deformation of the reinforced and unreinforced tunnel face are s_a and s_b respectively. If the rock mass deformation is to be controlled as u_m, the support structure with different stiffness is required. When the tunnel face does not have any reinforcement, the required tunnel support stiffness is k_b. When the tunnel face is reinforced, the required support stiffness is k_a. When there is no reinforcement on the tunnel face, the required tunnel support stiffness exceeds

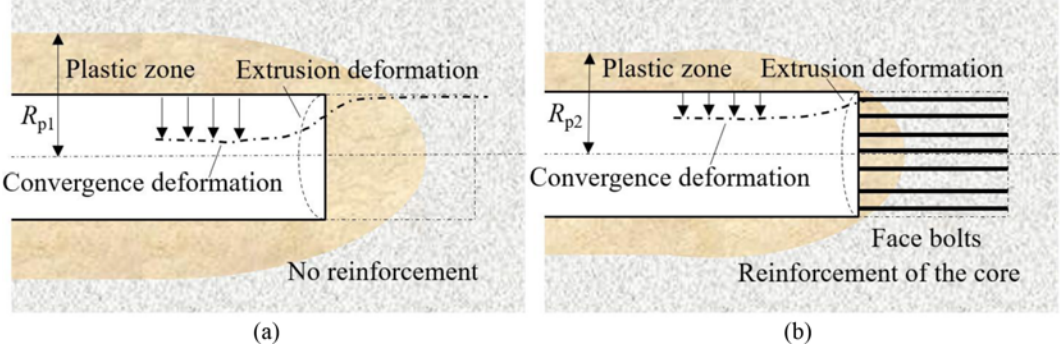

Fig. 1. Extrusion and Convergence Deformation of the Tunnel: (a) No Reinforcement, (b) Reinforcement of Core

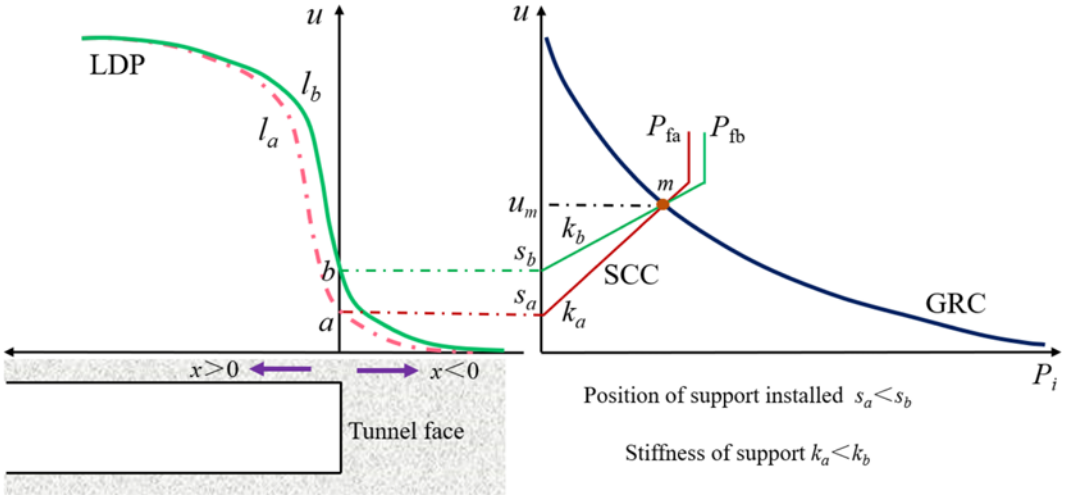

Fig. 2. Analysis of Rock-Support Interaction Under Different LDP

Table 1. Computational Models of LDP

Equation		Author	Research method
$u^*(x)=\frac{u_0(x)}{u_{omax}}=0.28+0.72\left[1-\left(\frac{0.84}{0.84+x^*}\right)^2\right](x\geq 0)$	(1)	Panet and Guenot (1983) (Panet and Guenot, 1983)	Numerical methods (Elastic)
$u^*(x)=\frac{u_0(x)}{u_{omax}}=0.25+0.75\left[1-\left(\frac{0.75}{0.75+x^*}\right)^2\right](x\geq 0)$	(2)	Panet (1995) (Panet, 1995)	Numerical methods (Elastic)
$u^*(x)=\frac{u_0(x)}{u_{omax}}=0.29+0.71\left\{1-\exp\left[-1.5\left(x^*\right)^{0.7}\right]\right\}(x\geq 0)$	(3)	Corbetta et al. (1991) (Corbetta et al., 1991)	Numerical methods (Elastic)
$u_0^*=0.22v+0.19\quad(x=0)$ $u^*(x)=\frac{u_0(x)}{u_{cos\,x}}=u_0^*+A_a\left[1-\exp\left(B_a x^*\right)\right]\quad(x\leqslant 0)$ $u^*(x)=\frac{u_0(x)}{u_{cos\,x}}=u_0^*+A_0\left[1-\left(\frac{B_0}{B_0+x^*}\right)^2\right]\quad(x\geqslant 0)$ $A_0=-0.22v-0.19;B_2=0.73v+0.81$ $A_0=-0.22v+0.81;B_b=0.39v+0.65$	(4)	Unlu and Gercek (2003) (Unlu and Gercek, 2003)	Numerical methods (Elastic)
$u^*(x)=\frac{u_0(x)}{u_{omar}}=\frac{1}{2}\left[1-\tanh\left(\frac{1}{3}-\frac{x^*}{2}\right)\right]$	(5)	Lee (1994) (Lee, 1994)	Empirical methods (Mathematical Statistics)
$u^*(x)=\frac{u_0(x)}{u_{omax}}=\left[1+\exp\left(-x^*/1.10\right)\right]^{-1.7}$	(6)	Hoek (1980) (Chern et al., 1998)	Empirical methods (Mathematical Statistics)
$u_0^*=\frac{1}{3}\exp\left(-0.15R^*\right)\quad(x=0)$ $u^*(x)=\frac{u_0(x)}{u_\infty}=u_0^*\exp\left(x^*\right)\quad(x\leqslant 0)$ $u^*(x)=\frac{u_0(x)}{u_\infty}=1-\left(1-u_0^*\right)\exp\left(-1.5x^*/R^*\right)\quad(x\geqslant 0)$	(7)	Vlachopoulos and Diederichs (2009) (Vlachopoulos and Diederichs, 2009)	Numerical methods (Elastic-perfectly plastic, elastic-brittle plasticity, strain-softening)
$u_0(x)/r_i=\begin{cases}d_1RMR^{d_2}d_3^{\left(x^*/2\right)} & (x<0)\\ d_4RMR^{d_5}\left(x^*/2\right)^{d_6} & (x>0)\end{cases}$	(8)	Basarir et al. (2010) (Basarir et al., 2010)	Numerical methods (Elastic-perfectly plastic)
$u^*=\frac{p_1+p_2BQ+p_3x^*}{1+p_4BQ+p_5x^*+p_6\left(x^*\right)^2}\quad(x<0)$ $u^*=\frac{p_1+p_2BQ+p_3BQ^2+p_4x^*+p_5\left(x^*\right)^2}{1+p_6BQ+p_7BQ^2+p_8x^*+p_9\left(x^*\right)^2}\quad(x\geq 0)$	(9)	Wu et al. (2015) (Wu et al., 2015)	Numerical methods (Elastic-perfectly plastic)

the tunnel support stiffness with the tunnel face reinforcement, i.e., $k_b > k_a$. In the tunnel support design, if the tunnel face reinforcement is neglected, the design value of the tunnel support stiffness will be large. When the tunnel face reinforcement is not considered, the support stiffness is larger, but its deformation is smaller. When considering the tunnel face reinforcement, the support stiffness is small, but its deformation is relatively large. In this case, the design of the bearing capacity of the tunnel support should be decided according to the support deformation and the corresponding stiffness together. If the ultimate bearing capacity is the same ($P_{fa} = P_{fb}$), the parameters of the tunnel support considering the tunnel face reinforcement than the tunnel face without the reinforcement. For the design of the tunnel support structure, the engineering economy is better when considering the tunnel face reinforcement.

It can be seen that the accurate determination of the point of the tunnel support installation is of greatly significance for the structure design. For this reason, there have been many studies on the LDP conducted by researchers. Table 1 shows some typical research results about the LDP.

Table 1 shows that many computational models of LDP have been proposed by researchers. But there are great differences in the number of variables, application objects, the scope of application, and research methods of different computational models of LDP. Among them, the LDP based on the maximum plastic zone radius proposed by Vlachopoulos and Diederichs (V-D (09)) is widely used. But the elastic-perfectly plastic material used in V-D (09) computational model. Subsequently, Rodriguez-Dono et al. (Rodriguez-Dono et al., 2010; Alejano et al., 2012; Vlachopoulos et al., 2013) extended the application range of V-D (09) and verified the correctness and applicability of V-D (09) for elastic-brittle plastic and strain-softening material. However, the V-D (09) disregards the tunnel face reinforcement effect. When the tunnel face is reinforced with reinforcement measures, the V-D (09) has a large calculation error, especially when the distance is close to the tunnel face. Therefore, the computational model of LDP considering the reinforcement of the tunnel face is studied in this paper.

3. Computational Model of LDP Considers the Effect of Tunnel Face Reinforced

3.1 Establishment of the Computational Model

In can be seen in the Fig. 3 that the tunnel face extrusion deformation and convergence deformation of rock mass is caused when the tunnel is excavated. Among them, the convergence deformation of rock mass composed of three parts, i.e. the deformation in the forward part of the tunnel face (pre-convergence, $x < 0$), at the tunnel face ($x = 0$), and behind the tunnel face (convergence, $x > 0$). According to the law of conservation of mass, there is a geometric transformation relationship between the tunnel face extrusion deformation and pre-convergence deformation at the tunnel face.

In this paper, there is an assumption that the volume expansion of the rock mass is not considered after the tunnel excavation

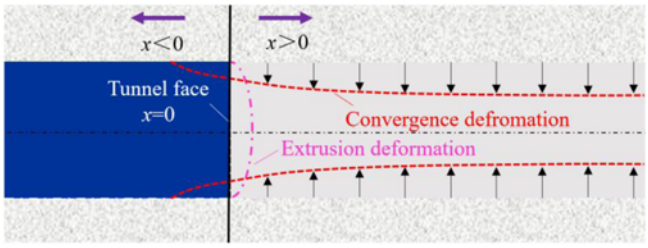

Fig. 3. Extrusion and Convergence Deformation of Tunnel

disturbance. According to the principle of volume equivalent, as shown in Eq. (10), the conversion calculation expression (Eq. (11)) between the tunnel face extrusion deformation and pre-convergence deformation is established:

$$V_3 = V_1 - V_2 \tag{10}$$

$$u_{r0} = \frac{3LR - \sqrt{(3LR)^2 - 4LR^2 u_e}}{2L} \tag{11}$$

The normalization of pre-convergence deformation can be obtained from the Eq. (11), as shown in Eq. (12):

$$u_{r0}^* = \frac{3LR - \sqrt{(3LR)^2 - 4LR^2 u_e}}{2Lu_\infty} \tag{12}$$

Combined with Eq. (9), the calculation expression of the LDP is:

$$\begin{cases} u_{r0}^* = \dfrac{3LR - \sqrt{(3LR)^2 - 4LR^2 u_e}}{2Lu_\infty} & (x = 0) \\ u_r^*(x) = \dfrac{u_r(x)}{u_\infty} = u_{r0}^* \exp\left(x^*\right) & (x \leqslant 0) \\ u_r^*(x) = \dfrac{u_r(x)}{u_\infty} = 1 - \left(1 - u_{r0}^*\right)\exp\left(-1.5x^* / R^*\right) & (x \geqslant 0) \end{cases} \tag{13}$$

where V_1, V_2, and V_3 are the volume of the cylinder, the truncated cone and the cone, respectively, and their geometric relationships are shown in Fig. 4; R is the tunnel radius; L is the excavation disturbance range; u_e is the extrusion deformation; x is the distance from the tunnel face; u_{ro} is the pre-convergence deformation; u_∞, R_p are the maximum convergence deformation and the maximum plastic zone radius without supporting force, respectively. Among them, $R^* = R_p/R$, $x^* = x/R$.

The maximum deformation and the maximum plastic zone radius without supporting force can be obtained using the Eqs. (14) and (15) (Fenner, 1938):

$$R_p = \left[\frac{\left(p_0 + c \cdot \cot\varphi\right)(1 - \sin\varphi)}{c \cdot \cot\varphi}\right]^{\frac{1-\sin\varphi}{2c\sin\varphi}} R \tag{14}$$

$$u_\infty = \frac{1+v}{E}\left\{p_0 - c \cdot \cot\varphi\left[\left(\frac{R_p}{R}\right)^{\frac{2\sin\varphi}{-\sin\varphi}} - 1\right]\right\}\frac{R_p^2}{R} \tag{15}$$

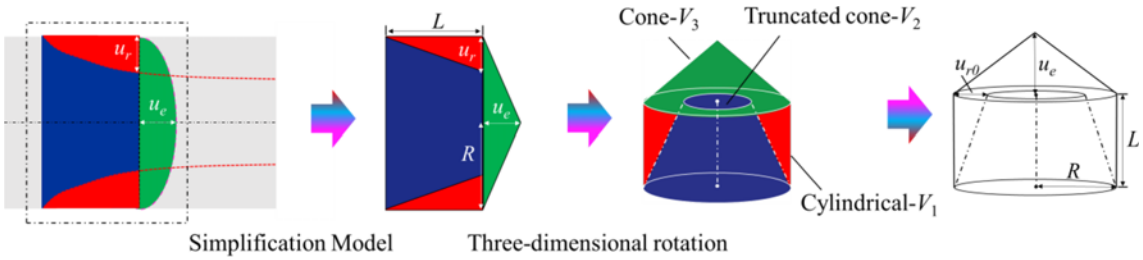

Fig. 4. Volume Equivalent Geometric Model

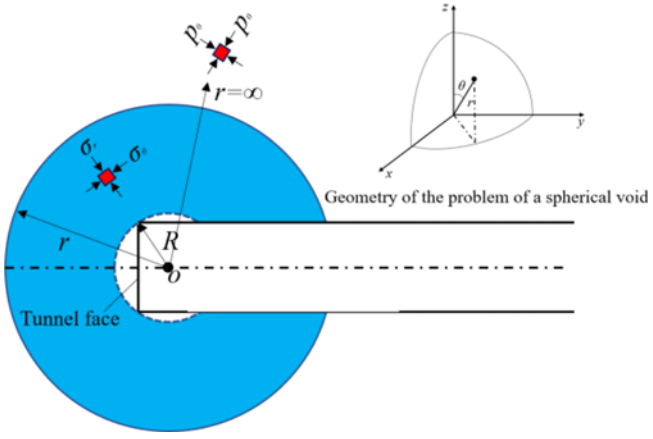

Fig. 5. A Computational Model of Tunnel Face Extrusion Deformation

The tunnel face extrusion deformation can be obtained using Eq. (16). It is proposed by Pierpaolo Oreste (Oreste, 2013) based on the spherical symmetry hypothesis. The calculation model is shown in Fig. 5.

$$u=\frac{n}{k+1}r-\frac{l}{k+m+1}r^{m+1}+\left[u_{R_{pi}}R_p^k-\frac{n}{k+1}R_p^{k+1}+\frac{l}{k+m+1}R_p^{m+k+1}\right]r^{-k} \tag{16}$$

$$\frac{R_{fp}}{R}=\left[\left(\frac{1.5p_0-f_{\text{penk}}}{N_{\text{peak}}+0.5}+\frac{f_{\text{res}}}{N_{\text{res}}-1}\right)/\left(p_{fi}+\frac{f_{\text{res}}}{N_{\text{res}}-1}\right)\right]^{\frac{1}{2(N_{\text{res}}-1)}}$$

$$n=\frac{f_{\text{res}}}{E}\left[(k-kv-2v)-\frac{1-kv+N_{\text{res}}(k-kv-2v)}{N_{\text{res}}-1}\right]+\frac{p_0}{E}(2kv-k+2v-1)$$

$$l=-\frac{p_{fi}+\left(\frac{f_{res}}{N_{res}-1}\right)}{E}\frac{1}{R^m}\left[1-kv+N_{res}(k-kv-2v)\right]$$

$$m=2\left(N_{\text{res}}-1\right)$$

$$k=\frac{1+\sin\psi}{1-\sin\psi}$$

$$u_{R_{fp}}=\frac{1+v}{2E}\left(p_0-\sigma_{r,R_p}\right)R_{fp}$$

$$\sigma_{r,R_{\text{fp}}}=\frac{1.5p_0-f_{\text{peak}}}{N_{\text{peak}}+0.5}$$

$$f_{\text{peak}}=\frac{2c_{\text{peak}}\cos\varphi_{\text{peak}}}{1-\sin\varphi_{\text{peak}}}$$

$$N_{\text{peak}}=\frac{1+\sin\varphi_{\text{peak}}}{1-\sin\varphi_{\text{peak}}}$$

$$f_{\text{res}}=\frac{2c_{\text{res}}\cos\varphi_{\text{res}}}{1-\sin\varphi_{\text{res}}}$$

$$N_{\text{res}}=\frac{1+\sin\varphi_{\text{res}}}{1-\sin\varphi_{\text{res}}}$$

where c_{peak} is the peak cohesion; φ_{peak} is the friction angle; c_{res} is the residual cohesion; φ_{res} is the residual friction angle; v is Poisson's ratio; v is dilatancy angle; E is Young's modulus; P_0 is the in-situ stress; R_{fp} is the tunnel face plastic zone radius; p_{fi} is the supporting force of tunnel face.

3.2 Parameter Determination

3.2.1 Extrusion Deformation of Tunnel Face under the Reinforced with Face Bolts

Due to its unique physical and mechanical properties, the face bolt is a commonly used support type for face reinforcement under weak rock mass geological conditions (Kamata and Mashimo,

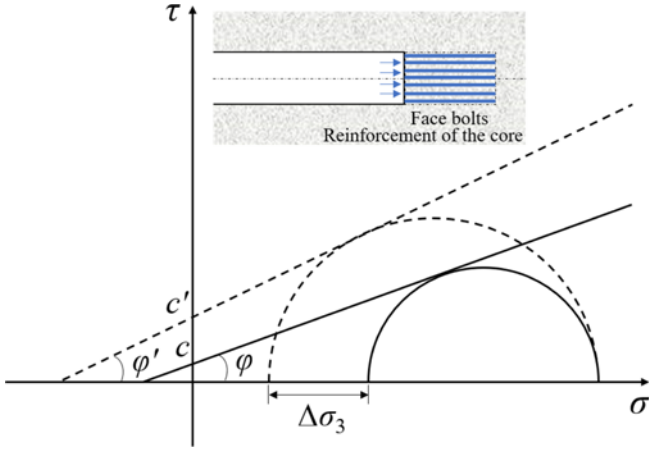

Fig. 6. Reinforcement Mechanism of Tunnel Face

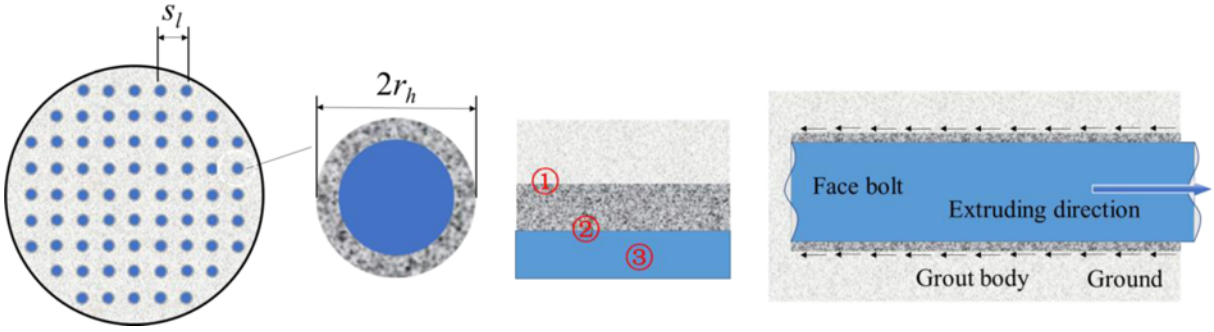

Fig. 7. The Failure Modes of the Tunnel Face Bolt

2003; Prisco et al., 2017). When the tunnel face is reinforced with face bolts, the interaction between the rock mass and the face bolts can increase the third principal stress, that is, the shear strength and stiffness of the rock mass at the tunnel face is increased, as shown in Fig. 6. Thereby, the tunnel face extrusion deformation can be reduced and the stability of the tunnel face can be enhanced.

The literature (Zhang et al., 2020a; Zhang et al., 2020b, 2020c) pointed out that the face bolt can fail in three different ways, which are the shear failure at the interface between the grouting body and the rock mass (①), the shear failure at the interface between the grouting body and the bolt body (②) and the tensile failure (③) of the bolt body, as shown in Fig. 7.

However, the test shows (Paternesi et al., 2017) that the failure model ① is more likely to occur than the failure model ② and the failure model ③. Therefore, it is assumed in this paper that only the failure model ① occurs in the face bolt. And it is assumed that the face bolts are evenly arranged and the interface shear strength remains the same under the given rock mass conditions.

The calculation expression of the face bolt support force p_{fi} can be expressed as (Paternesi et al., 2017):

$$p_{fi} = \frac{2\pi r_h l_b \tau_s}{s_l^2} \tag{17}$$

where l_b is the lap length of the face bolt; S_l is the spacing of the face bolt; τ_s is the shear strength of the grouting body-rock mass interface; r_h is the radius of the grouting hole.

When the tunnel face is reinforced by the face bolt, the u_{pe} under the reinforcement of the face bolt can be obtained through the relevant calculation model (see Section 3.1). By replacing u_e in Eq. (13), the calculation formula of the longitudinal deformation curve considering the action effect of the face bolt can be obtained.

3.2.2 Excavation Disturbance Range of Tunnel Face

Numerous research results (Lee and Schubert, 2008; Anagnostou and Perazzelli, 2015; Pan and Dias, 2017) show that the fracture surface in front of the tunnel face is a logarithmic spiral, as shown in Fig. 8. The angle β between the bottom of the failure surface and the horizontal direction is equal to $\pi/4 + \varphi/2$, and the height of the face is $2R$.

Basing on the Fig. 8, the calculation expression of the excavation

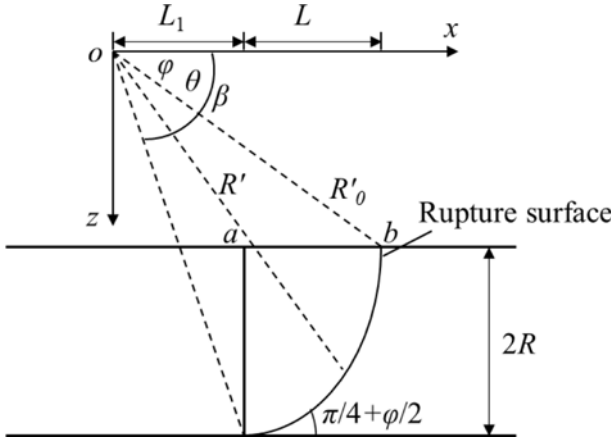

Fig. 8. Calculation Model for the Disturbance Range of Tunnel Excavation

disturbance range L of the tunnel face is:

$$L = \cos\varphi R_0^{'} - L_1 \tag{18}$$

The equation of the failure logarithmic spiral curve in front of the tunnel face is:

$$R^{'} = R_0^{'} e^{(\theta-\varphi)\tan\varphi} \tag{19}$$

$$R_0^{'} = \frac{2R}{\sin\beta e^{(\beta-\varphi)\tan\varphi} - \sin\varphi}$$

$$L_1 = \cos\beta R_0^{'} e^{(\beta-\varphi)\tan\varphi}$$

where R'_0 is the length of ob; L_1 is the horizontal distance from point o to point a; L is the horizontal distance from point a to point b, that is, the excavation disturbance range of the face; β is the clamp between oc and x-axis. There is an angle between any radius and the x-axis called θ ($\varphi \le \theta \le \beta$).

3.3 Validation

3.3.1 Theoretical Verification

A comparison between the proposed model and the V-D (09) model is presented here to validate the proposed model's accuracy. To highlight the accuracy of related derivation and calculation, this paper simplifies the rock mass mechanical parameters. That is, if

there is no special explanation in the analysis, there is an assumed that the peak strength parameter equals the residual strength parameter, and the dilatancy of the rock mass is not considered. An overview of all calculation parameters can be found in Table 2.

The calculation results of the two calculation models under different parameters are shown in Fig. 9.

In Fig. 9, along with increasing P_0, the slope of the curve decreases, and the results of the two models agree well. In the proposed model and V-D (09), the average difference between the results is approximately 6.4%. And the u_{r0}^* hardly changes with R. The difference under different R is the same as 2.6%. As can be seen from this paper, the proposed model is reasonable.

Table 2. Calculated Parameters

Symbol	Variables
P_0 (MPa)	1, 2, 3, 4, 5
c_p (MPa)	0.5
c_r (MPa)	0.5
φ_p (°)	30
φ_r (°)	30
E (GPa)	1
μ	0.25
R (m)	3, 5, 7, 9

3.3.2 Numerical Verification

To ensure that the proposed model is rational, the FLAC^{3D} which is the finite difference software is used for 5 analyses. This section provides an overview of the simulations using the finite difference software, and the calculation parameters is provided in Table 2.

Extrusion deformations of a reinforced tunnel face with varying support forces of the tunnel face are studied. The numerical model used in this study calculates the maximum extrusion deformation value at the tunnel face as the calculated value. It can be seen from the Fig. 10 that the displacement at the center point (point A) of the tunnel face.

Mohr-Coulomb's failure criterion is supposed to apply to the ground as it is an elastic-plastic material. A mathematical model

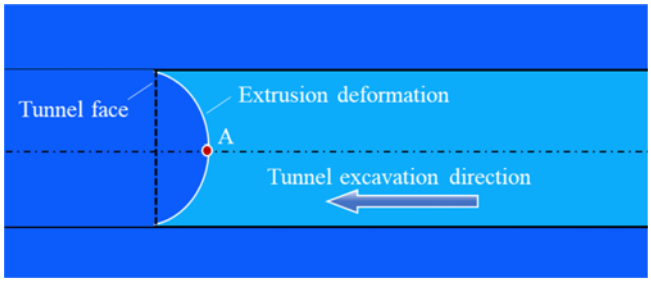

Fig. 10. Schematic Diagram of Tunnel Excavation

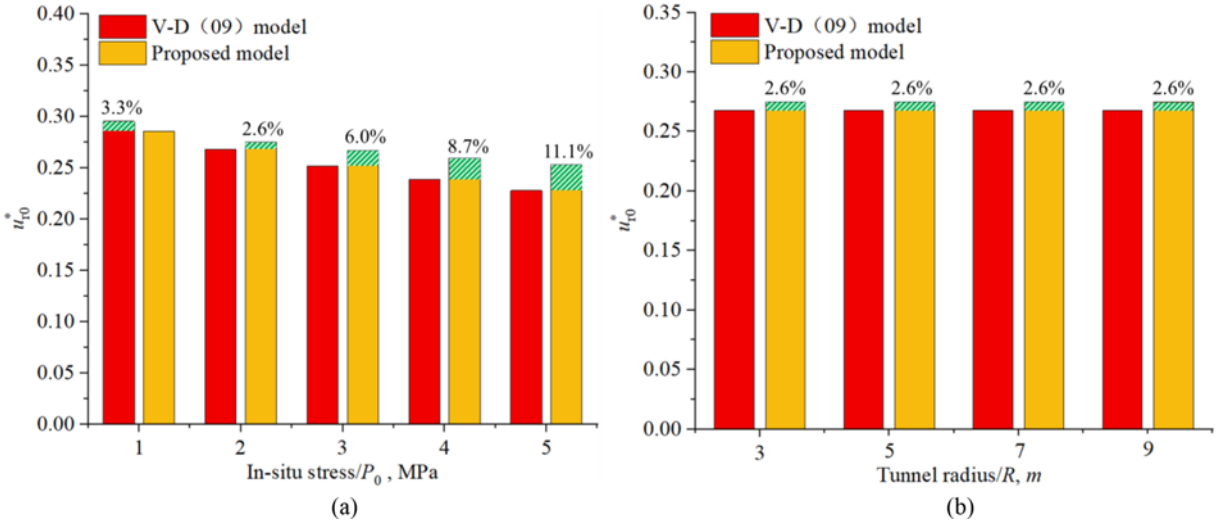

Fig. 9. Analyzing the Result of the Proposed Model and V-D (09) Model: (a) In-Situ Stress P_0, (b) Tunnel Radius R

Table 3. Calculating Parameters of the Numerical Model

Tunnel		Ground		Support force	
Symbol	Value	Symbol	Value	Symbol	Value
R (m)	3	P_0 (MPa)	3	p_{fi} (MPa)	1.13,0.28,0.13,0.07,0.045
		c (MPa)	0.5		
		φ (°)	30		
		E (GPa)	1		
		v	0.25		

is shown in Fig. 11 along with its boundary conditions (case of tunnel radius R = 3 m). To directly focus on the extrusion deformation, the FLAC^{3D} model considers the following simplified tunnel excavation process:

1. Setting up the in situ stress condition.
2. Removing excavation materials and excavating.
3. Installation of the tunnel face support force.
4. Calculation of the extrusion deformation.

Table 4 indicates that the pre-convergence increases with increasing the p_{fi}. When the p_{fi} are 1.13 MPa, 0.28 MPa, 0.13 MPa, 0.07 MPa, 0.045 MPa, respectively, the relative difference of proposed model and numerical model about normalized pre-convergence of tunnel face are 4.58%, 3.48%, 2.21%, 2.12%, 5.37%, respectively. A difference of 3.55% exists between the numerical model and the proposed model. It appears that the model proposed in this paper is reasonable.

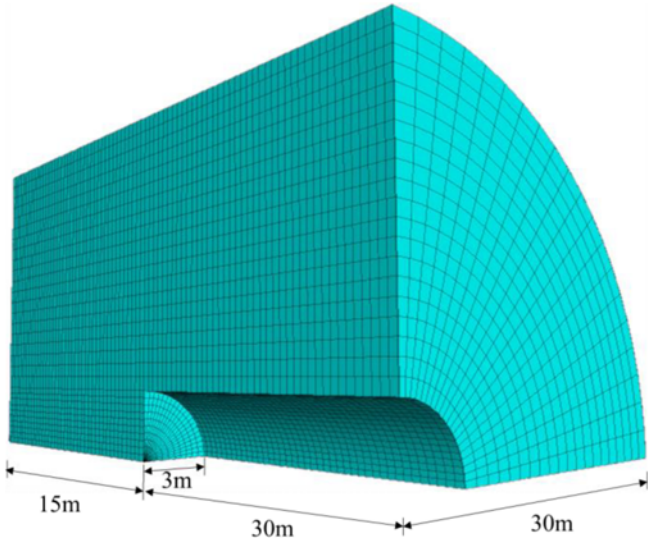

Fig. 11. Computational Domain and Boundary Conditions

Table 4. The Relative Difference of Proposed Model and Numerical Model

Support force (MPa)	Method		Relative difference
	Numerical model	Proposed model	
1.13	0.125	0.131	4.58%
0.28	0.208	0.201	3.48%
0.13	0.231	0.226	2.21%
0.07	0.241	0.236	2.12%
0.045	0.255	0.242	5.37%

This paper demonstrates that the proposed model is reasonable by comparing it to a theoretical calculation model and a numerical calculation model. For the tunnel face's stability, many existing soft rock tunnels have adopted advanced reinforcement measures. However, its effect on LDP is less considered, and even LDP without reinforcement is still used to design tunnel support. The design parameters for tunnel supports will undoubtedly be affected by this.

Although there are many types of advance support, but limited to the research conditions, only the extrusion deformation of tunnel faces under tunnel face bolt reinforcement is studied in this paper. For this reason, the generalization of the model proposed is limited. However, from the research direction, the research results proposed in this paper promote the further development of LDP. Further, it can expand the application field of CCM and has great research value.

4. Parameter Analyses and Discussion

4.1 Effect of Face Bolts on LDP

According to the above analysis, the LDP is greatly affected by the extrusion deformation of the tunnel face. The tunnel face with reinforcement affects the extrusion deformation of the tunnel face. Therefore, the variation law of LDP under the reinforcement by face bolts is analyzed in this section. A summary of the calculating parameters can be found in Table 5.

Figure 12 indicates that the pre-convergence increases with increasing the spacing of face bolts. When the spacing of face bolts are 0.5 m, 1.0 m, 1.5 m, 2.0 m, 2.5 m, respectively, the normalized pre-convergence of tunnel face are 0.131, 0.201, 0.226, 0.236, 0.242, respectively. When the face bolts spacing increases to 2.5 m, the control effect of tunnel face reinforcement on pre-convergence is poor. Compared with the pre-convergence without reinforcement, it is only reduced by 0.98%. As can be seen, in order to reduce the tunnel face extrusion deformation and the pre-convergence, the face bolt density must be increased.

4.2 Effect of Face Bolts on Convergence Deformation of the Rock Mass

When the CCM is used to design the tunnel support, the location

Table 5. Calculating Parameters

Tunnel		Ground		Face bolts	
Symbol	Value	Symbol	Value	Symbol	Value
R (m)	5	P_0 (MPa)	3	l_b (m)	6
		c (MPa)	0.5	S_l (m)	0.5,1.0,1.5,2.0,2.5
		φ (°)	30	τ_s (kPa)	60
		E (GPa)	1	r_h (m)	0.125
		v	0.25		

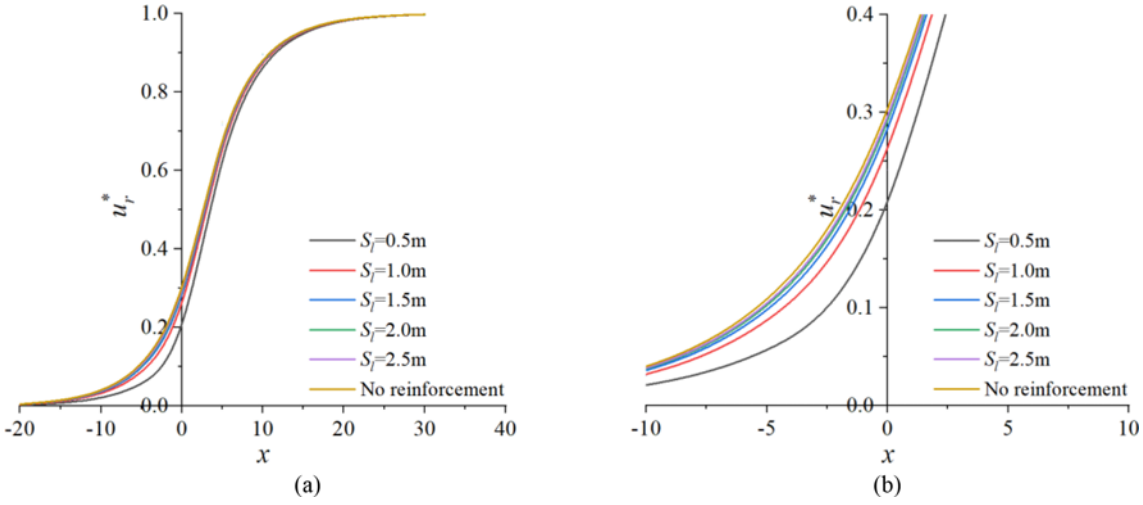

Fig. 12. The Normalized LDP for Different Spacing of Face Bolts: (a) LDP, (b) LDP-Local Amplification

Table 6. Calculating Parameters

Tunnel		Ground		Face bolts		Primary support	
Symbol	Value	Symbol	Value	Symbol	Value	Symbol	Value
R (m)	5	P_0 (MPa)	4	l_b (m)	6	K_s (GPa/mm)	0.1
		c (MPa)	0.4	S_l (m)	0.5,1.0,1.5		
		φ (°)	25	τ_s (kPa)	100		
		E (GPa)	1	r_h (m)	0.125		
		v	0.25				

of the tunnel support installed is depended on the LDP, and the different location of the tunnel support installed influences greatly on the convergence deformation. Hence, the convergence deformation under the reinforcement of the tunnel face is analyzed by cases. Table 6 summarizes the reinforcement and geotechnical parameters. Assuring the tunnel's safety during construction requires the provision of primary support (Prazeres et al., 2012; Taromi et al., 2016; Niedbalski et al., 2018). Its main supporting components include rock bolts, steel rib, shotcrete, and reinforcement mesh. This calculation is a simplified analysis, without considering the single action of each support component, and assuming that the primary support stiffness is a certain value.

Figure 13 shows the normalized final tunnel displacement with different spacing (S_l) of face bolts. The normalized final tunnel displacement increases with the increased spacing (S_l). When the spacing of face bolts is 0.5 m, 1.0 m, and 1.5 m, respectively, the normalized final tunnel displacement is 0.27, 0.29, and 0.32, respectively. Normalized final tunnel displacement is reduced when the tunnel face is reinforced compared to no reinforcement. It is evident that the tunnel face reinforcement has an important impact on controlling the final tunnel displacement. Conversely, if the support design is based on controlling the tunnel displacement, the required support stiffness increases. When the spacing of the face bolts is 0.5 m and the support stiffness is K_s, the final tunnel displacement is u_1. Then when the same type of support is used, if the final tunnel deformation is

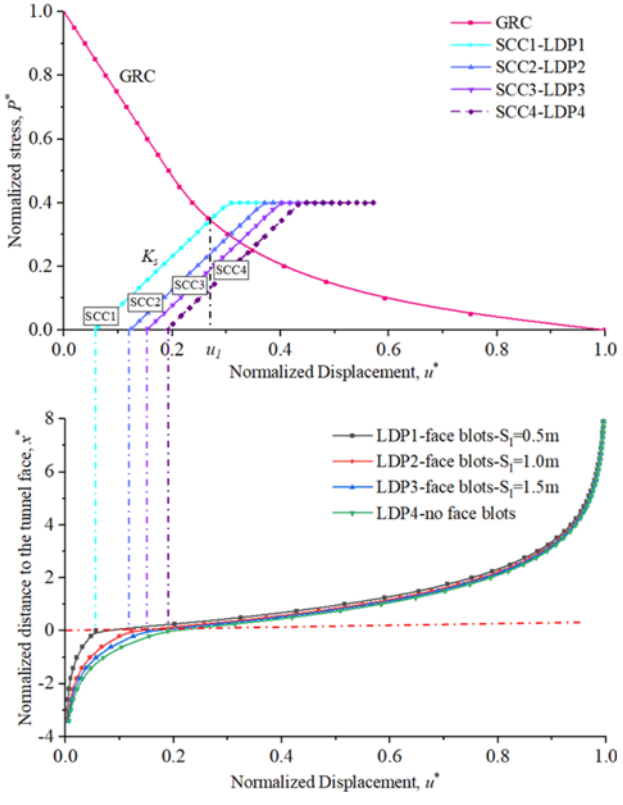

Fig. 13. Convergence Deformation of Ground Under Different Tunnel Face Reinforcement Strength

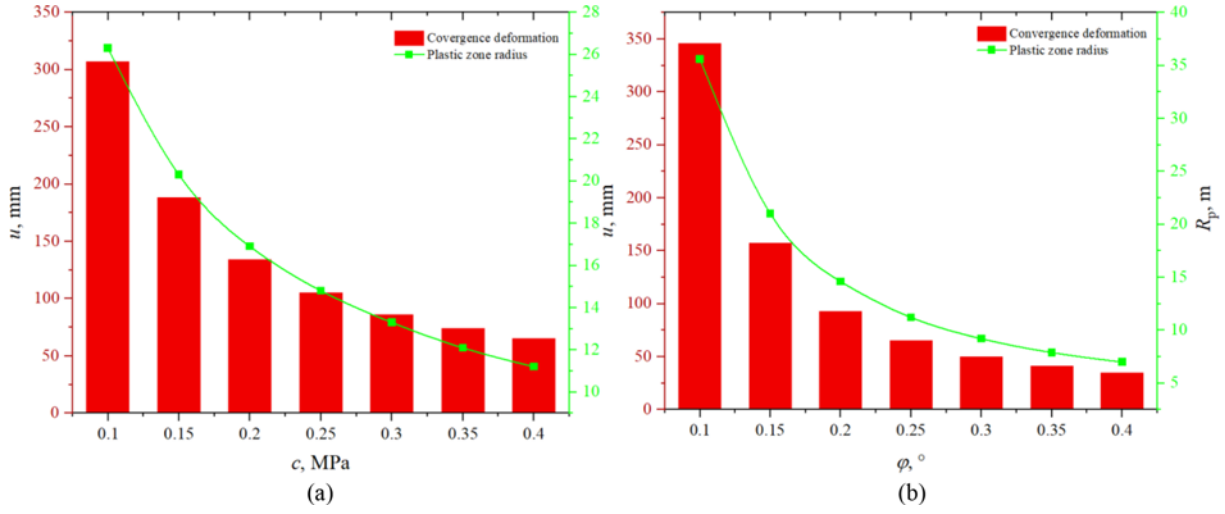

Fig. 14. Influence of the Mechanical Parameters on the Convergence Deformation and the Plastic Zone Radius: (a) Different Cohesion, (b) Different Friction (other parameters be found in Table 6)

controlled to u_1, the support stiffness needs to be increased at this time. The support stiff in this case should be greater than K_s. Otherwise, it will not achieve the expected control result about the final tunnel displacement. And with the weakening of the tunnel face reinforcement effect, the required tunnel support stiffness increases.

According to the analysis of the elastic-plastic analytical solution (Fenner, 1938), as shown in Fig. 14, there is a higher correlation between mechanical parameters of the ground and deformations associated with convergence, and the larger the convergence deformation the weaker the mechanical parameters of the ground.

At the same time, combined with the above analysis results can be seen that the tunnel face reinforcement can effectively attenuate the weakening of the mechanical parameters of the ground, further ensuring the stability of the ground. Therefore, it is important to consider the reinforcement effect of the tunnel face when designing the tunnel support. However, the existing support structure design using the CCM doesn't consider the reinforcement effect of the tunnel face. But the study results proposed in this paper can provide new ideas for designing the support structure.

As a geological body, the rock mass is in a stable equilibrium until it is disturbed by the outside world. The excavation of the tunnel has destroyed the original equilibrium of the cavern wall due to the loss of support from the original rock mass. And to the hole space expansion and deformation, thus changing the relative equilibrium of adjacent masses, causing the adjustment of stress, strain and energy to reach a new equilibrium, this redistribution of the stress field is called the secondary stress field.

The stress state after redistribution is call redistributed stress state, and the rock within the influence of redistributed stress is called the surrounding rock. For the elastic rock with linear stress-strain relationship, it is usually assumed that it can withstand very high stress without damage, and the excavation of the tunnel produces stress relief, resulting the radial stress around the hole becomes zero and the tangential stress is concentrated. The rock mass beyond the perimeter of the cave, which is approximately double the diameter of the tunnel, gradually returns to its initial stress state. As for elastic-plastic rock mass, the tress-strain relationship is nonlinear. When the tangential stress around the hole reaches the yield condition of the rock mass, the rock mass becomes the plastic state, leading to the appearance of the plastic zone. Thus, the stress is continuously transferred to the deep part of the rock mass and deformation occurs at the same time, when this deformation exceeds the capacity of the rock mass itself, the rock mass will be damaged.

The secondary stress field in the rock mass is actually three-dimensional. Due to the stress release and deformation development of the tunnel face on the rock mass have a great restraint effect, so that along the tunnel longitudinal sections on the secondary stress state and deformation are not the same, this phenomenon is called support space effect of tunnel face. The tunnel face spatial effect allows the rock mass within a certain area near the tunnel face to be stabilized in an unsupported situation. Tunnel excavation construction is a complex four-dimensional space-time problem, and the influence of time and space on the development of deformation and stability of the rock mass is again crucial.

During the tunnel construction process, the stress and deformation of the rock mass is partly caused by the gradual release of load as the tunnel face moves forward, and partly caused by the creep of the rock mass as it grows over time (Cheng et al., 2021; Cheng et al., 2022; Lyu et al., 2022). Because of the large disturbance of the rock mass during the tunnel excavation construction, the space effect provided by the rock mass at the tunnel face plays a significant role in ensuring the stability of the unsupported rock mass at the tunnel face. And it also plays a better virtual support role for the rock mass stability in the support section. However, the existing design method doesn't consider the spatial effect under the effect of the tunnel face reinforcement, so it should be paid attention to in the actual engineering.

6. Conclusions

A model for calculating the LDP considering reinforcement of the tunnel face is developed in this paper based on the principle of equivalent volume, because of the inadequacy of the existing model for calculating the LDP without considering the tunnel face reinforcement. The following conclusions were mainly obtained from the analysis:

1. Comparing the results calculated by the proposed model and V-D (09), the average difference is approximately 6.4%. This results in a very good agreement between the proposed model and the V-D (09). So, the proposed model meets the requirements of engineering calculation.
2. When tunnel face support forces are applied, the final convergence deformation of the rock mass can be effectively reduced. If the reinforcement effect of the tunnel face is ignored, the tunnel's finally deformation value will be overestimated. Ultimately, this leads to the consequences of higher design parameters of the tunnel support and poor engineering construction economy. But the model proposed in this paper overcomes this deficiency.

Acknowledgments

This work was supported by the Project of China Railway Science and Technology Research and Development Plan (Grant No. P2019G038-5).

ORCID

Not Applicable

References

Alejano L, Rodriguez-Dono A, Veiga M (2012) Plastic radii and longitudinal deformation profiles of tunnels excavated in strain-softening rock masses. *Tunnelling and Underground Space Technology incorporating Trenchless Technology Research* 30:169-182, DOI: 10.1016/j.tust.2012.02.017

Alejano L, Rodriguez-Dono A, Alonso E, Fdez-Manin G (2009) Ground reaction curves for tunnels excavated in different quality rock masses showing several types of post-failure behaviour. *Tunnelling and Underground Space Technology incorporating Trenchless Technology Research* 24:689-705, DOI: 10.1016/j.tust.2009.07.004

Anagnostou G, Perazzelli P (2015) Analysis method and design charts for bolt reinforcement of the tunnel face in cohesive-frictional soils. *Tunnelling and Underground Space Technology incorporating Trenchless Technology Research* 47:162-181, DOI: 10.1016/j.tust.2014.10.007

Basarir H, Genis M, Ozarslan A (2010) The analysis of radial displacements occurring near the face of a circular opening in weak rock mass. *International Journal of Rock Mechanics & Mining Sciences* 47:771-783, DOI: 10.1016/j.ijrmms.2010.03.010

Barla G (2016) Full-face excavation of large tunnels in difficult conditions. *Journal of Rock Mechanics and Geotechnical Engineering,* 10, DOI: 10.1016/j.jrmge.2015.12.003

Cantieni L, Anagnostou G, Hug R (2011) Interpretation of core extrusion measurements when tunnelling through squeezing ground. *Rock Mechanics & Rock Engineering* 44:641-670, DOI: 10.1007/s00603-011-0170-5

Carranza-Torres C, Fairhurst C (2000) Application of the Convergence-Confinement method of tunnel design to rock masses that satisfy the Hoek-Brown failure criterion. *Tunnelling and Underground Space Technology incorporating Trenchless Technology Research* 15:187-213

Cheng L, Jla B, Yi R, Chao L, Yin Z (2022) Mechanical characteristics and permeability evolution of salt rock under thermal-hydro-mechanical (THM) coupling condition. *Engineering Geology* 302, DOI: 10.1016/j.enggeo.2022.106633

Cheng L, Liu J, Ren Y, Liang C, Liao Y (2021) Study on very long-term creep tests and nonlinear creep-damage constitutive model of salt rock. *International Journal of Rock Mechanics and Mining Sciences* 146:104873, DOI: 10.1016/j.ijrmms.2021.104873

Chern JC, Shiao FY, Yu CW (1998) An empirical safety criterion for tunnel construction

Corbetta F, Bernaud D, Nguyen-Mihn D (1991) Contribution à la méthode convergence-confinement par le principe de la similitude. *Revue Francaise De Geotechnique* 54:5-11

Cui L, Sheng Q, Zheng J, Cui Z, Shen Q (2019) Regression model for predicting tunnel strain in strain-softening rock mass for underground openings. *International Journal of Rock Mechanics and Mining Sciences* 119:81-97, DOI: 10.1016/j.ijrmms.2019.04.014

Fenner R (1938) Untersuchungen zur erkenntnis des gebirgsdrucks. *Glückauf* 32:681-695

Hoek E (1980) Underground excavations in rock. Underground Excavations in Rock

Kabwe E, Karakus M, Chanda E (2019) Proposed solution for the ground reaction of non-circular tunnels in an elastic-perfectly plastic rock mass - ScienceDirect. Computers and Geotechnics 119

Kamata H, Mashimo H (2003) Centrifuge model test of tunnel face reinforcement by bolting, DOI: 10.1016/s0886-7798(03)00029-4

Lee Y (1994) Prise en compte des non-linéarités de comportement des sols et des roches dans la modélisation du creusement d'un tunnel

Lee Y, Schubert W (2008) Determination of the round length for tunnel excavation in weak rock. *Tunnelling & Underground Space Technology Incorporating Trenchless Technology Research* 23:221-231, DOI: 10.1016/j.tust.2007.04.001

Lunardi P (2008) Design and construction of tunnels. Design & Construction of Tunnels, 79

Luo Y, Chen J, Chen Y, Diao P, Qiao X (2018) Longitudinal deformation profile of a tunnel in weak rock mass by using the back analysis method. *Tunnelling and Underground Space Technology* 71:478-493, DOI: 10.1016/j.tust.2017.10.003

Lyu C, Liu J, Ren Y, Liang C, Zhang Q (2022) Study on long-term uniaxial compression creep mechanical behavior of rocksalt-mudstone combined body. *International Journal of Damage Mechanics* 31:275-293, DOI: 10.1177/10567895211035488

Niedbalski, Z, Malkowski P, Majcherczyk T (2018) Application of the NATM method in the road tunneling works in difficult geological conditions - The Carpathian flysch. *Tunnelling and Underground Space Technology* 74:41-59, DOI: 10.1016/j.tust.2018.01.003

Oke J, Vlachopoulos N, Diederichs M (2018) Improvement to the convergence-confinement method: Inclusion of support installation proximity and stiffness. Rock Mechanics & Rock Engineering

Oreste P (2003) Analysis of structural interaction in tunnels using the covergence–confinement approach. *Tunnelling & Underground Space*

Technology Incorporating Trenchless Technology Research 18:347-363, DOI: 10.1016/s0886-7798(03)00004-x

Oreste P (2008) Distinct analysis of fully grouted bolts around a circular tunnel considering the congruence of displacements between the bar and the rock. *International Journal of Rock Mechanics & Mining Sciences* 45:1052-1067, DOI: 10.1016/j.ijrmms.2007.11.003

Oreste P (2013) Face stabilization of deep tunnels using longitudinal fibreglass dowels. *International Journal of Rock Mechanics & Mining Sciences* 58:127-140, DOI: 10.1016/j.ijrmms.2012.07.011

Pan Q, Dias D (2017) Safety factor assessment of a tunnel face reinforced by horizontal dowels. *Engineering Structures* 142:56-66, DOI: 10.1016/j.engstruct.2017.03.056

Panet M (1995) Le calcul des tunnels par la méthode convergence-confinement. Presses de l'ecole nationale de Ponts et Chausse's, Paris

Panet M, Guenot A (1983) Analysis of convergence behind the face of a tunnel: Tunnelling 82, proceedings of the 3rd international symposium, Brighton, 7-11 June 1982, P197-204. Publ London: IMM, 1982. *International Journal of Rock Mechanics & Mining Sciences & Geomechanics Abstracts* 20:A16-A16

Paternesi A, Schweiger H, Scarpelli G (2017) Numerical analyses of stability and deformation behavior of reinforced and unreinforced tunnel faces. *Computers & Geotechnics* 88:256-266, DOI: 10.1016/j.compgeo.2017.04.002

Prazeres PG, Thoeni K, Beer G (2012) Nonlinear analysis of NATM tunnel construction with the boundary element method. *Computers & Geotechnics* 40:160-173, DOI: 10.1016/j.compgeo.2011.10.005

Prisco C, Flessati L, Frigerio G, Castellanza R, Caruso M, Galli A, Lunardi P (2017) Experimental investigation of the time-dependent response of unreinforced and reinforced tunnel faces in cohesive soils. Acta Geotechnica, DOI: 10.1007/s11440-017-0573-x

Rodriguez-Dono A, Alejano L, Veiga M (2010) Analysis of longitudinal deformation profiles using Flac3D, ISRM International Symposium 2010 and 6'" Asian Rock Mechanics Symposium - Advances in Rock Engineering

Song F, Rodriguez-Dono A, Olivella S, Zhong Z (2020) Analysis and modelling of longitudinal deformation profiles of tunnels excavated in strain-softening time-dependent rock masses. *Computers and Geotechnics* 125:103643, DOI: 10.1016/j.compgeo.2020.103643

Taromi M, Eftekhari A, Hamidi J, Aalianvari A (2016) A discrepancy between observed and predicted NATM tunnel behaviors and updating: A case study of the Sabzkuh tunnel. Bulletin of Engineering Geology & the Environment 1-17, DOI: 10.1007/s10064-016-0862-x

Unlu T, Gercek H (2003) Effect of Poisson's ratio on the normalized radial displacements occurring around the face of a circular tunnel. *Tunnelling and Underground Space Technology Incorporating Trenchless Technology Research* 18:547-553, DOI: 10.1016/S0886-7798(03)00086-5

Vlachopoulos N, Diederichs MS (2009) Improved longitudinal displacement profiles for convergence confinement analysis of deep tunnels. *Rock Mechanics and Rock Engineering* 42:131-146

Vlachopoulos N, Diederichs M, Marinos V, Marinos P (2013) Tunnel behaviour associated with the weak Alpine rock masses of the Driskos Twin Tunnel system, Egnatia Odos Highway. *Canadian Geotechnical Journal* 50:91-120, DOI: 10.1139/cgj-2012-0025

Wang H, Nie G (2010) Analytical expressions for stress and displacement fields in viscoelastic axisymmetric plane problem involving time-dependent boundary regions. *Acta Mechanica* 210:315-330, DOI: 10.1007/s00707-009-0208-x

Wu S, Gen X, Gao Y, Zhao G, Li J, Yan Q (2015) A study of the longitudinal deformation of tunnels based on the generalized Hoek-Brown failure criterion. *Rock and Soil Mechanics* 36:946-952+987, DOI: 10.16285/j.rsm.2015.04.005

Zhang Q, Jiang B, Wang S, Ge X, Zhang H (2012) Elasto-plastic analysis of a circular opening in strain-softening rock mass. *International Journal of Rock Mechanics and Mining Sciences* 50:38-46, DOI: 10.1016/j.ijrmms.2011.11.011

Zhang Q, Wang H, Jiang Y, Lu M, Jiang B (2019) A numerical large strain solution for circular tunnels excavated in strain- softening rock masses. *Computers and Geotechnics* 114, DOI: 10.1016/j.compgeo.2019.103142

Zhang X, Wang M, Li J, Wang Z, Liu D (2020a) Safety factor analysis of a tunnel face with an unsupported span in cohesive-frictional soils. *Computers and Geotechnics* 117:103221, DOI: 10.1016/j.compgeo.2019.103221

Zhang X, Wang M, Wang Z, Li J, Liu D (2020b) A limit equilibrium model for the reinforced face stability analysis of a shallow tunnel in cohesive-frictional soils. *Tunnelling and Underground Space Technology* 105:103562, DOI: 10.1016/j.tust.2020.103562

Zhang X, Wang M, Wang Z, Li J, Liu D (2020c) Stability analysis model for a tunnel face reinforced with bolts and an umbrella arch in cohesive-frictional soils. *Computers and Geotechnics* 124:103635, DOI: 10.1016/j.compgeo.2020.103635

Zhou Z, Cai X, Li X, Cao W, Du X (2020) Dynamic response and energy evolution of sandstone under coupled static–dynamic compression: Insights from experimental study into deep rock engineering applications. *Rock Mechanics and Rock Engineering* 53:1305-1331, DOI: 10.1007/s00603-019-01980-9